JOURNAL OF GEOPHYSICAL RESEARCH, VOL. 115, A07321, doi:10.1029/2009JA014461, 2010

Ionospheric response to the initial phase of geomagnetic storms: Common features

Wenbin Wang,[1,2] Jiuhou Lei,[3] Alan G. Burns,[1] Stanley C. Solomon,[1] Michael Wiltberger,[1] Jiyao Xu,[2] Yongliang Zhang,[4] Larry Paxton,[4] and Anthea Coster[5]

Received 13 May 2009; revised 15 March 2010; accepted 25 March 2010; published 29 July 2010.

[1] Ionospheric responses to the initial phases of three geomagnetic storms: 2–5 April 2004, 7–9 November 2004, and 13–16 December 2006, were compared using both ground-based GPS total electron content (TEC) data and coupled magnetosphere ionosphere thermosphere (CMIT) model simulations. The onset times for these storms all occurred at local daytime in the North American sector. This similarity of onset times and other factors resulted in some common features in their ionospheric response. These common features include (1) enhanced TEC (positive response) at low and middle latitudes in the daytime, (2) depleted TEC (negative response) around the geomagnetic equator in the daytime, (3) a north-south asymmetry in the positive response as the northern hemispheric response appeared to be more pronounced, and (4) negative response at high latitudes as the storms progressed. The CMIT model captured most of these features. Analysis of model results showed that storm-time enhancements in the daytime eastward electric field were the primary cause of the observed positive storm effects at low and middle latitudes as well as the negative response around the geomagnetic equator in the daytime. These eastward electric field enhancements were caused by the penetration of high latitude electric fields to low latitudes during southward interplanetary magnetic field (IMF) periods, when IMF B_z oscillated between southward and northward direction in the initial, shock phase of the storms. Consequently, the ionosphere was lifted up at low and middle latitudes to heights where recombination was weak allowing the plasma to exist for a long period resulting in higher densities. In addition, the CMIT model showed that high-latitude negative storm responses were related to the enhancements of molecular nitrogen seen in TIMED/Global Ultraviolet Imager observations, whereas the negative storm effects around the geomagnetic equator were not associated with thermospheric composition changes; they were the result of plasma transport processes.

Citation: Wang, W., J. Lei, A. G. Burns, S. C. Solomon, M. Wiltberger, J. Xu, Y. Zhang, L. Paxton, and A. Coster (2010), Ionospheric response to the initial phase of geomagnetic storms: Common features, *J. Geophys. Res.*, *115*, A07321, doi:10.1029/2009JA014461.

1. Introduction

[2] Geomagnetic storms usually have three phases after the sudden storm commencement (SSC): the initial phase, main phase, and the recovery phase [e.g., *Gonzalez et al.*, 1994; *Prölss*, 1995]. The response of the thermosphere-ionosphere (T-I) system to energy and momentum inputs from the solar wind plasma, and interplanetary magnetic field (IMF) and the magnetosphere during storms involve nonlinear interactions of dynamical, chemical, and electrodynamical processes of different temporal and spatial scales [e.g., *Fuller-Rowell et al.*, 1994; *Burns et al.*, 1995; *Prölss*, 1995; *Buonsanto*, 1999; *Mendillo*, 2006, and references therein]. At each phase of a storm, different processes and their nonlinear interactions play different roles depending on geophysical conditions, resulting in significant global and local variations of this response that have solar cycle, season, local time, and UT dependences [*Prölss*, 1995; *Burns et al.*, 2004a; *Mendillo*, 2006]. Fully understanding the effect of all these processes and their interactions on the complex response of the T-I system to storms remains one of the major challenges in the ionospheric physics [e.g., *Prölss*, 1995; *Buonsanto*, 1999; *Mendillo*, 2006; *Burns et al.*, 2007].

[3] While there have been many descriptions of ionospheric and thermospheric behavior during the initial phases

[1]High Altitude Observatory, National Center for Atmospheric Research, Boulder, Colorado, USA.
[2]State Key Laboratory of Space Weather, Chinese Academy of Sciences, Beijing, China.
[3]Aerospace Engineering Sciences Department, University of Colorado at Boulder, Boulder, Colorado, USA.
[4]Applied Physics Laboratory, Johns Hopkins University, Laurel, Maryland, USA.
[5]Haystack Observatory, Massachusetts Institute of Technology, Westford, Massachusetts, USA.

0148-0227/10/2009JA014461

of the storms in the literature, most storm research so far has been focused on the main and recovery phases of the storms. Both positive (enhanced electron density) and negative (depleted electron density) ionospheric responses have been observed during the initial phases of the storms [e.g., *Adeniyi*, 1986; *Abdu et al.*, 1991, 1995; *Lakshmi et al.*, 1991; *Abdu*, 1997; *Mendillo*, 2006; *Yizengaw et al.*, 2006]. Many authors have shown evidence that penetration electric fields can cause daytime electron density and total electron content (TEC) enhancements at low and middle latitudes soon after storm commencements [e.g., *Jakowski et al.*, 1992; *Lin et al.*, 2005; *Mannucci et al.*, 2005; *Zhao et al.*, 2005; *Mendillo*, 2006, and references therein]. In contrast, *Prölss et al.* [1991] and *Prölss* [1993, 1995] proposed that traveling atmospheric disturbances are the main cause of the daytime positive response after storm commencements. It is important to note that most of these studies were limited to specific locations or regions and thus lacked a global perspective.

[4] The use of a few stations at specific locations also made it difficult for these studies to separate the effects of commencement time, solar wind and IMF conditions, season, solar cycle, longitude, and other geophysical conditions on the response of the T-I system to geomagnetic storms and to study the commonality and differences between storms as well as the physical processes that result in these storm properties. In recent years, more and more GPS TEC data have become available. This has allowed global maps of ionospheric TEC to be developed and has thus allowed storm effects to be investigated on a global scale. In this study we will use these global TEC maps and a physics-based, coupled, global magnetosphere, ionosphere, and thermosphere model to study the commonalities and differences of the ionospheric response to the initial phases of three storms and the physical processes that cause these commonalities and differences.

[5] In addition to positive storm effects, negative storm effects are found at the geomagnetic equator and high/middle latitudes during mostly the main and recovery phases of storms [*Abdu*, 1997; *Cander and Mihajlovic*, 2005]. Negative storm effects at high latitudes are caused mainly by thermospheric composition changes because of the upwelling of molecular rich air to higher altitudes driven by the enhanced Joule heating that occurs during storms [*Mayr et al.*, 1978; *Burns et al.*, 1991; *Fuller-Rowell et al.*, 1994]. Negative storms effects at middle latitudes can be caused by the extension of the composition change zone into this region as a result of changes in the neutral wind circulation that are driven by the increased storm-time forcing at high latitudes. They can also occur simply because of the movement of main ionospheric trough region to lower latitudes because of the expansion of the auroral region [*Prölss et al.* 1991; *Blagoveshchensky et al.*, 2005]. The negative storm effects around the geomagnetic equator are more closely related to changes in transportation, although composition changes can be effective there at later times during strong storms [*Prölss*, 1995; *Buonsanto*, 1999].

[6] As *Field et al.* [1998] and *Szuszczewicz et al.* [1998] pointed out, an accurate, fully physics-based, self-consistent model of the upper atmosphere is needed to fully understand the global response of the thermosphere and ionosphere during all phases of geomagnetic storms. Most previous model simulations use either empirical low latitude dynamo models [e.g. *Richmond et al.*, 1980], empirical high latitude convection models or observed electric fields, and sometimes empirical neutral wind models to drive ionospheric models. Thus, the dynamical, electrodynamical, and chemical coupling between the thermosphere, ionosphere, and magnetosphere is not self-consistently calculated in these simulations [e.g., *Rasmussen and Greenspan*, 1993; *Swisdak et al.*, 2006; *Romanova et al.*, 2008]. Recently, a coupled magnetosphere, thermosphere, and ionosphere (CMIT) model has been developed. This model simulates a global ionospheric electric field, which includes the neutral wind dynamo, the high latitude electric field of magnetospheric origin, and penetration electric fields self-consistently, in addition to the dynamical and chemical processes within the coupled thermosphere-ionosphere system [*Wang et al.*, 2004; *Wiltberger et al.*, 2004, *Wang et al.*, 2008]. *Wang et al.* [2008] compared the CMIT-simulated ionospheric vertical drifts with those measured by the Jicamarca incoherent scatter radar for the 2–5 April 2004 storm and obtained the same temporal variations between observations and model results. They showed that there was a significant, long-duration penetration of high latitude electric fields to lower latitudes and that these penetration electric fields occurred even during quiet times, as long as there were temporal changes in the high-latitude electric fields. *Lei et al.* [2008] used the CMIT model to study the ionospheric response to the initial phase of the 13–16 December 2006 storm event and found that the structure of the modeled global ionospheric storm response is the same as that in GPS TEC observations.

[7] In this paper we focus on the global response of the ionosphere to the initial phase of three storms that began at roughly the same UT. The response of the ionosphere to geomagnetic storms has been found to be closely related to the commencement time of each storm [e.g., *Prölss*, 1993, 1995]. However, it is not clear, at present, what the differences and similarities of the ionospheric response are if storms commence at the same time. In this study we will compare ionospheric responses to the initial phase of three geomagnetic storms: 2–5 April 2004, 6–9 November 2004, and 13–16 December 2006, which had roughly the same sudden storm commencement (SSC) times but otherwise occurred in different geophysical conditions. We will show the commonality, as well as the differences, between these storms and investigate the causes of these characteristics.

[8] In the next section, we will describe briefly CMIT and the sources of data that were used to drive the model. We will then give global GPS TEC changes during the initial phases of these storms and compare them with CMIT model simulations that self-consistently calculate global ionospheric electric fields. Discussion of the characteristics of these responses and their causes will be given in sections 4 and 5. Conclusions will then be drawn in section 6.

2. Model Description

[9] The CMIT model couples the Lyon-Fedder-Mobarry (LFM) global magnetosphere magnetohydrodynamic (MHD) code [*Lyon et al.*, 2004] with the thermosphere ionosphere electrodynamics general circulation model (TIEGCM) [*Richmond et al.*, 1992]. The LFM magnetospheric code solves the ideal magnetohydrodynamic (MHD) equations for the magnetosphere in a conservative form using the partial

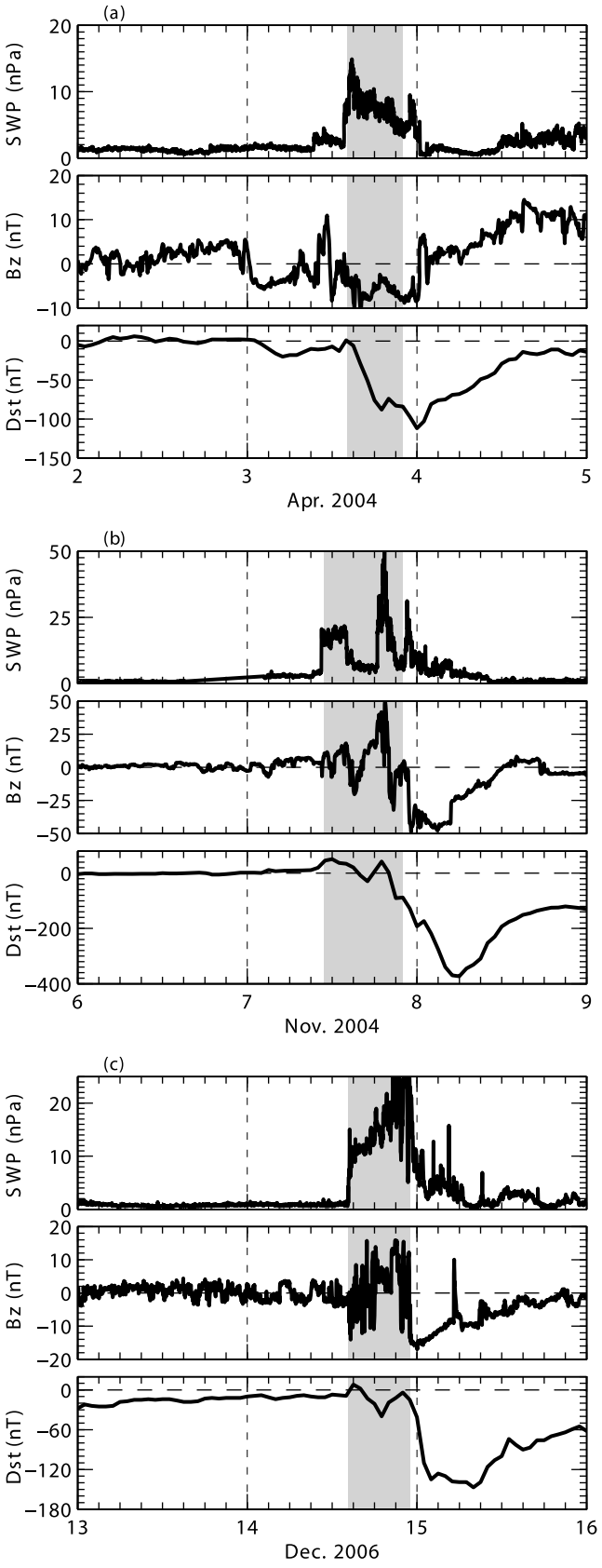

interface method on a distorted spherical mesh and Yee-type grid [*Lyon et al.*, 2004]. The TIEGCM [*Roble et al.*, 1988; *Richmond et al.*, 1992] is a time-dependent, 3-D model that solves the fully coupled, nonlinear, hydrodynamic, thermodynamic, and continuity equations of the thermospheric neutral gas self-consistently with the ion continuity equations using a finite differencing scheme. In the CMIT model, these two codes are coupled by exchanging parameters across their interfaces through a magnetosphere-ionosphere (M-I) coupler module. These parameters include field-aligned currents, auroral precipitation from the LFM code, and neutral wind induced currents and ionospheric conductance from the TIEGCM. A detailed description of the coupling procedure is given by *Wiltberger et al.* [2004] and *Wang et al.* [2004].

[10] The coupling between the magnetospheric global MHD codes and the thermosphere ionosphere global circulation models (GCMs) replaces empirical models of high-latitude convection electric fields and auroral precipitation. This enables studies of the dynamical coupling between the magnetosphere and ionosphere and thus the impact of the solar wind/magnetosphere on the ionosphere variability to be made. CMIT has the ability to self-consistently simulate a global ionospheric electric field that includes both the imposed high latitude electric field from the magnetosphere and dynamo electric field generated by thermospheric winds. It can also simulate penetration electric fields induced by the rapid changes in solar wind and IMF conditions [*Wang et al.*, 2008].

3. Results

3.1. Solar Wind and IMF Conditions

[11] The solar wind and interplanetary magnetic field (IMF) data that were used as boundary conditions to drive CMIT in this study were shown in Figure 1. The solar wind and IMF data for the 2–5 April and 6–9 November 2004 events were measured by the ACE satellite [*Stone et al.*, 1998], whereas those during the 13–16 December 2006 event were from Wind satellite observations [*Acuña et al.*, 1995], since there was a data gap in the ACE data for this event [*Lei et al.*, 2008].

[12] Figure 1 shows solar wind dynamic pressures, IMF B_z and *Dst* values for the 2–5 April 2004 (Figure 1a), 6–9 November 2004 (Figure 1b), and 13–16 December 2006 (Figure 1c) events, respectively. The shaded areas are the time intervals in which the thermosphere/ionosphere responses to these solar wind/IMF conditions are discussed in this paper. The beginning of these intervals correspond to the SSC times for each storm and thus the significant jumps in solar wind dynamic pressure, a signature of the arrival of an interplanetary shock. These intervals corresponded to the initial or early main phases of the storms, as indicated by D_{st} changes in the bottom plots in Figures 1a–1c. We will simply refer to

Figure 1. Solar wind dynamic pressure (nPa), IMF B_z component (nT) and *Dst* index (nT) for (a) 2–4 April 2004, (b) 6–9 November 2004, and (c) 13–16 December 2006 storms, respectively. The data for the 2–4 April 2004 and 6–9 November 2004 storms were obtained from the ACE satellite measurements, those for the 13–16 December 2006 storm were from the Wind satellite measurements.

all of them as the initial phases throughout the rest of the paper.

[13] One common feature of these storms is that they started at roughly the same UT. For the April 2004 event the SSC time was at about 1410 UT, for the November 2004 case it happened at 1052 UT, and for the December 2006 case it happened at 1414 UT. Note here that for the November 2004 event, although the shock arrived and SSC began at 1052 UT, IMF B_z did not turn southward until 1400 UT. Thus, the significant impact by this storm on the thermosphere and ionosphere should have happened after 1400 UT, which was at roughly the same time as those in the other two storms. In Figure 1, solar wind and IMF data for all three events were shifted by about 30 min from their measurement times by the ACE and Wind satellites at the L1 point so that sudden jumps in solar wind pressures coincided with the SSC times. This delay was roughly the same as the propagation time of the shock from the L1 point to the magnetopause. Nevertheless, these storms began during post-dawn local times in the North American sector.

[14] The storms studied in this paper occurred in low, but variable, solar activity conditions. The 3 day averages of $F_{10.7}$ fluxes were 108.1, 125.1, and 88.5 for 2–5 April 2004, 6–9 November 2004, and 13–16 December 2006, respectively. Thus, there were differences in solar EUV radiation of about 16%–41% among these storms. Solar wind and IMF conditions were significantly different. First, the magnitudes and temporal variations of the solar wind dynamic pressures were different. For the April 2004 event, the solar wind dynamic pressure jumped from ~2 to about 15 nPa, it then rapidly decreased to below 10 nPa. For the December 2006 event, the solar wind dynamic pressure was above 10 nPa during the entire shock interval, with a maximum larger than 20 nPa. The solar wind dynamic pressure variations for the November 2004 event were more significant than for the other two events. Note that we used a different scale for the solar wind dynamic pressure for this storm (Figure 1b). The solar wind dynamic pressure jumped to about 20 nPa and stayed at roughly the same level for about 3 h. It then dropped rapidly to about 7 nPa. After that it had two large peaks, one occurred at about 1800 UT, with a maximum value of more than 50 nPa. Another peak occurred at the end of the initial phase at about 2100 UT, with a peak value of 30 nPa.

[15] The IMF B_z conditions were also very different for these storms. Again, the scale for the November 2004 storm is much larger than the other two. IMF B_z was almost entirely southward during the entire interval of the initial phase for the April 2004 event, oscillating between -4 and −8 nT. For the December 2006 event, B_z varied between ±10 nT in the first 3 h period. It then became completely northward for the next 4 h. At the end of this initial phase, B_z turned southward very rapidly and attained a minimum value of −17 nT. In the initial phase of the November 2004 event, B_z varied between a northward and southward direction, with a period of about 2–3 h. The amplitude of the oscillation became larger with time.

[16] Thus, the geophysical conditions for the initial phase of these three storms were significantly different. The magnetospheric ring current responses were also different, as shown by the observed *Dst* plots in Figure 1. The questions that need to be addressed here then are: With all these differences in solar radiation, season, solar wind, and IMF conditions, does the thermosphere-ionosphere system respond similarly or differently; and what are the physical processes that drive the similarities or differences in these storms?

3.2. Global TEC Observations

[17] Figure 2 shows four global maps of GPS TEC differences with respect to the quiet-time backgrounds (the day before the storm) for each storm from 1600 to 2225 UT, with an interval of 2 h. Significant ionospheric F_2 peak density changes are observed to occur usually 2–3 h later than SSC because electron density enhancements need time to build up [*Lei et al.*, 2008]. There were no noticeable differences between storm-time and quiet-time TECs for the first 2 h after SSC during these events. Thus, they are not included in Figure 2.

[18] Each TEC difference map in Figure 2 was obtained in a 25 min period to ensure enough data coverage. The GPS TEC data used were collected from the Madrigal database at the MIT Haystack Observatory (http://www.openmadrigal.org). A detailed description of the TEC data processing procedure was given by *Rideout and Coster* [2006]. The same color scales were used in these maps to allow easy comparisons. Figure 2 is plotted as a function of geographic latitude and local time, with local noon located in the middle of each plot. Thus, the world map shifts with UT in successive plots.

[19] Row A shows TEC differences for the period between 1600 and 1625 UT. This period corresponded to about 2 h after the SSC for the April 2004 and December 2006 storm events and about 5 h into the initial phase for the November 2004 event, but only 2 h after the southward turning of IMF B_z. Although the storm histories were not the same, the global morphology of the ionospheric response was about the same in this UT interval. For the April 2004 storm, positive storm effects (enhanced TEC or electron densities) occurred in the North American sector, Atlantic Ocean, and the west part of the Europe. In the Southern Hemisphere, positive storm effects happened in the South American and African regions. These enhanced TEC regions occurred at geomagnetically low and middle latitudes (about ±10° to ±50° geomagnetic latitude). There were no data available over the Pacific, Atlantic, and Indian oceans. Thus, it is difficult to obtain a global view of the storm-time TEC changes in the Southern Hemisphere. A negative storm effect (decrease in TEC) occurred along a narrow band around the geomagnetic equator (dotted lines in Figure 2).

[20] The middle plot of row A shows TEC changes during the November 2004 storm in the same time period (1600–1625 UT). Similar positive and negative distributions to those of the April 2004 storm are seen. That is, positive storm effects occurred at geomagnetically low and middle latitudes in both the northern and southern American sectors, as well as in the European sector. Negative response happened along the geomagnetic equator again (geomagnetic latitude lower than about ±10°). The December 2006 storm also had similar features, although the positive response was weaker than it was in the other two storms. The negative response was much stronger and occurred not only along the geomagnetic equator but also over a more widespread area, especially in the South American sector.

[21] Two hours later (Figure 2b), positive storm effects were enhanced for all three storms. These positive storm effects also occurred in roughly the same locations. In the Northern Hemisphere, positive effects extended from the

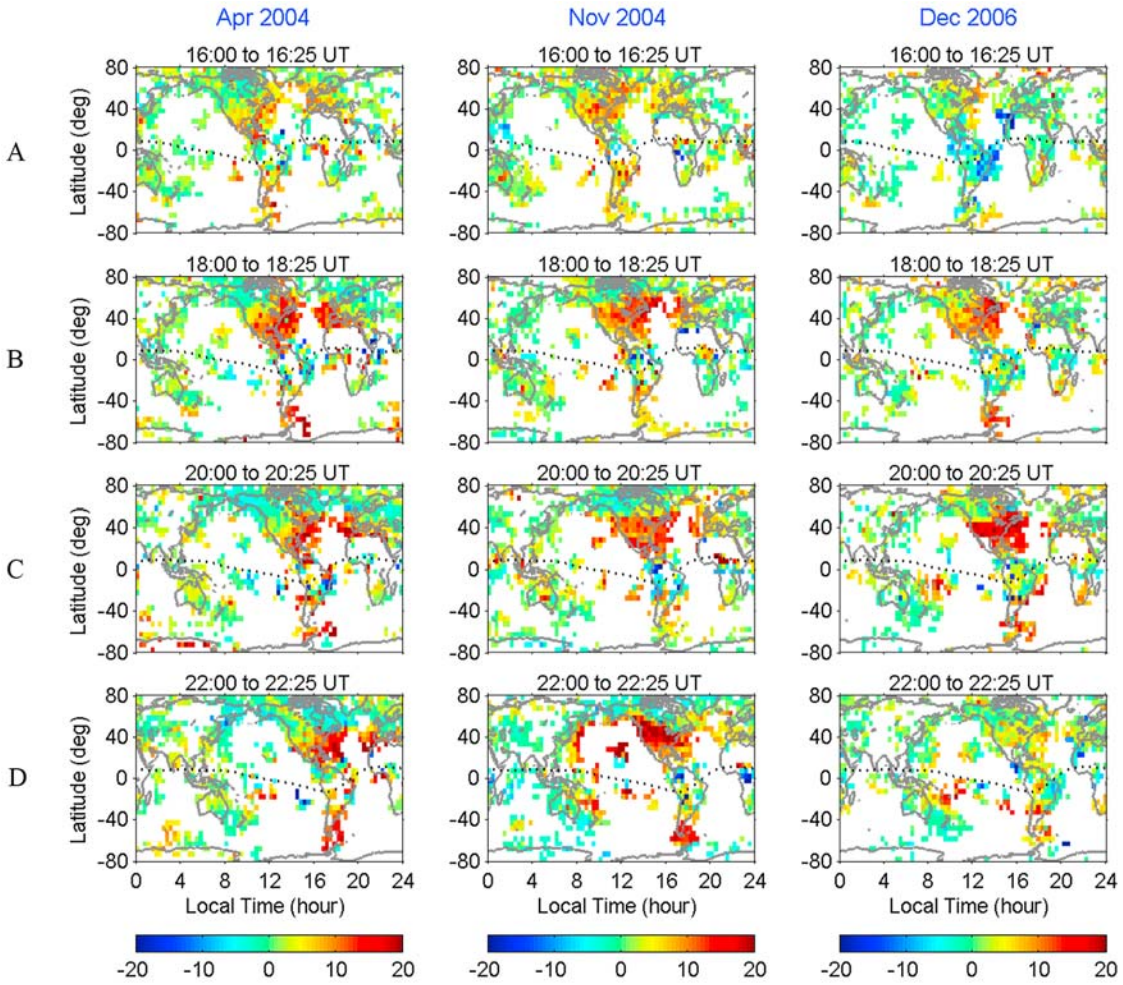

Figure 2. Global maps of differential GPS TEC between the disturbed day and quiet day (previous day) from 1600 to 2200 UT for April 2004 (left column), November 2004 (middle column), and December 2006 storm (right column), respectively. The unit of differential TEC is TECu (1 TECu = 10^{16} electrons/m^2).

west coast of the American sector to the west part of the Europe and from about 20° to 60° geomagnetic latitude. The magnitudes of TEC enhancements were also almost the same for the April 2004 and November 2004 storms over Eastern Europe. The increase of TEC in the December 2006 storm was not as large as it was in the other two storms in the Northern Hemisphere. In the Southern Hemisphere, positive storm effects were also evident at roughly the same locations for all three storms (i.e., at geomagnetically middle latitudes in the South American sector). The magnitudes of the TEC enhancements were weaker there for the November 2004 storm, compared with those at this location in the other two storms. The hemispheric asymmetry in the positive responses became more pronounced for all three storms. For the April 2004 and November 2004 storms, there were enhancements in the negative response at high latitudes: between ~0800 and ~1200 LT in the North American sector and between ~1600 and ~2000 LT in northern Europe.

[22] At 2000–2025 UT, positive storm effects persisted or were even enhanced in the North American sector for all three storms (Figure 2c). The most significant enhancement occurred in the December 2006 event. The locations of the positive storm effects were the same as they were 2 h earlier. In the Southern Hemisphere, positive storm effects remained very much the same as they were before. However, it appears that there was a significant enhancement in the storm-time TEC just east of Australia. This enhancement was more evident in the December 2006 storm. The negative storm effects along the geomagnetic equator for the three storms were also mainly the same as they were before. However, they were slightly stronger than they were in the previous plot in the April 2004 and November 2004 events. In addition, negative storm effects were also enhanced at high latitudes and extended into middle latitudes in both hemispheres (about ±50° in geomagnetic latitude).

[23] Figure 2d shows a different morphology for these three storms 2 h later, in the 2200–2225 UT interval. Positive storm effects in the April 2004 storm were similar to those at 2000–2025 UT in the North American sector. High-latitude negative storm effects were strengthened, extended to even lower latitudes, and covered wider areas in longitude. Positive storm effects were much stronger than they were at 2000–2025 UT for the November 2004 storm. They also became noticeable in the East Asian sector, as well as east of Australia. Positive storm effects were also strengthened in the South American sector. Negative storm effects were confined

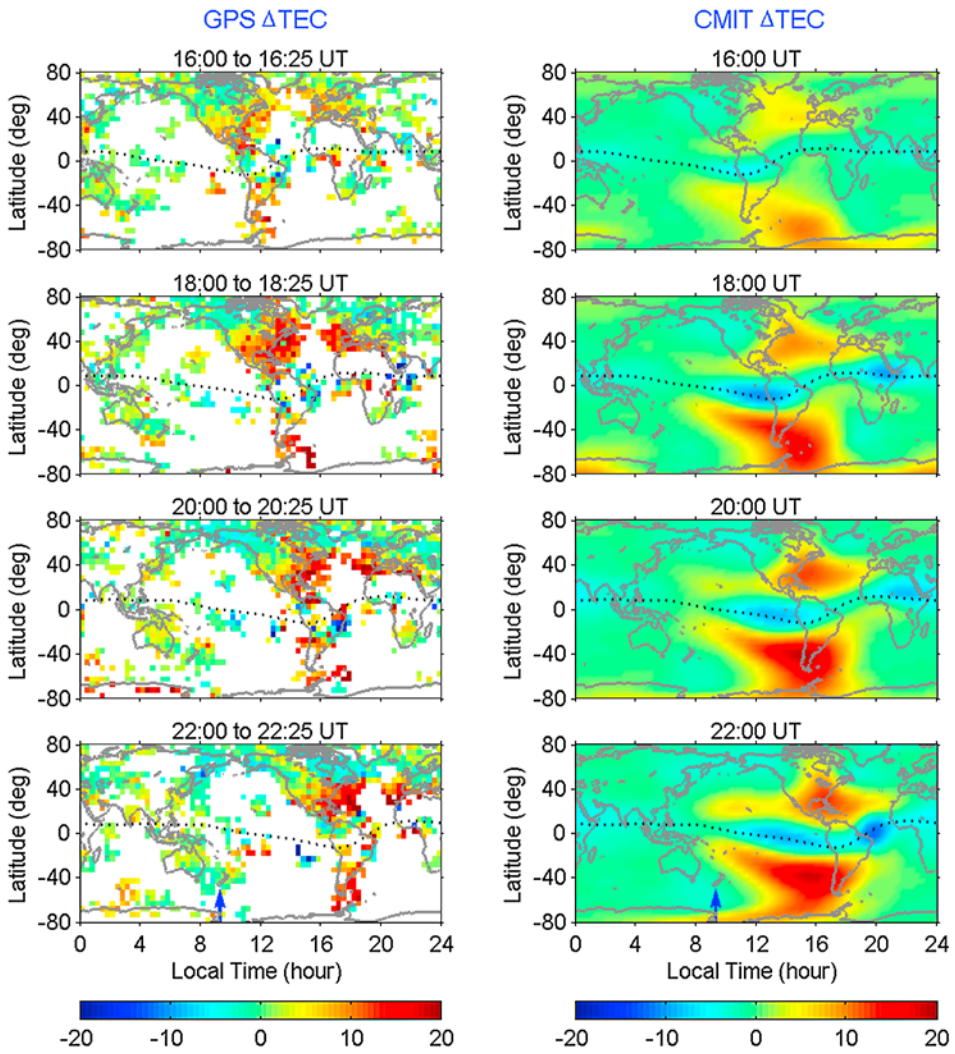

Figure 3. Global maps of differential (left) GPS TEC and (right) CMIT-simulated TEC between the disturbed day (3 April) and quiet day (2 April) from 1600 to 2200 UT for the April 2004 storm. The unit of differential TEC is TECu (1 TECu = 10^{16} electrons/m^2).

to the daytime high latitudes in the North American sector and early morning in the middle Asian and European sectors. Negative storm effects in the Southern Hemisphere, however, clearly became stronger, especially over the west Australia and Antarctic regions. As for the December 2006 storm, positive storm effects were significantly weakened globally, and this weakening was more evident in the Northern Hemisphere.

[24] More common features than differences were seen in these storms during their initial phases, even though they were under very different solar radiation, seasonal, solar wind, and IMF conditions. These common features include (1) positive storm effects at geomagnetically middle and low latitudes in both hemispheres in the daytime, (2) negative storm effects along the geomagnetic equator, (3) the extension of high-latitude negative storm effects to lower latitudes as storm progresses in the daytime, and (4) north-south hemispheric asymmetry in both positive and negative storm effects. However, because of the limitations in available observations in the Southern Hemisphere, it was difficult to have a very clear picture of the north-south asymmetry of the ionospheric response to storms, although there was strong evidence for this asymmetry in the TEC differential maps.

3.3. CMIT Model Simulations

[25] The common features that were seen in the ionospheric response to the initial phases of different geomagnetic storms suggest that the physical processes that drive these responses are fundamental ones in the ionosphere and thermosphere system and that they should be represented in physics-based, first principle models. In this section we show results from simulations of the coupled magnetosphere ionosphere thermosphere (CMIT) model to test this idea. If the model results are consistent with observations, a diagnostic analysis of the model outputs should reveal the physical processes that produced the observed ionospheric behavior during the initial phases of all three storms.

[26] Figure 3 shows a comparison between the observed TEC changes and CMIT-simulated ones for the initial phase of the April 2004 storm. The left column shows the GPS TEC difference maps that were already given in Figure 2, whereas

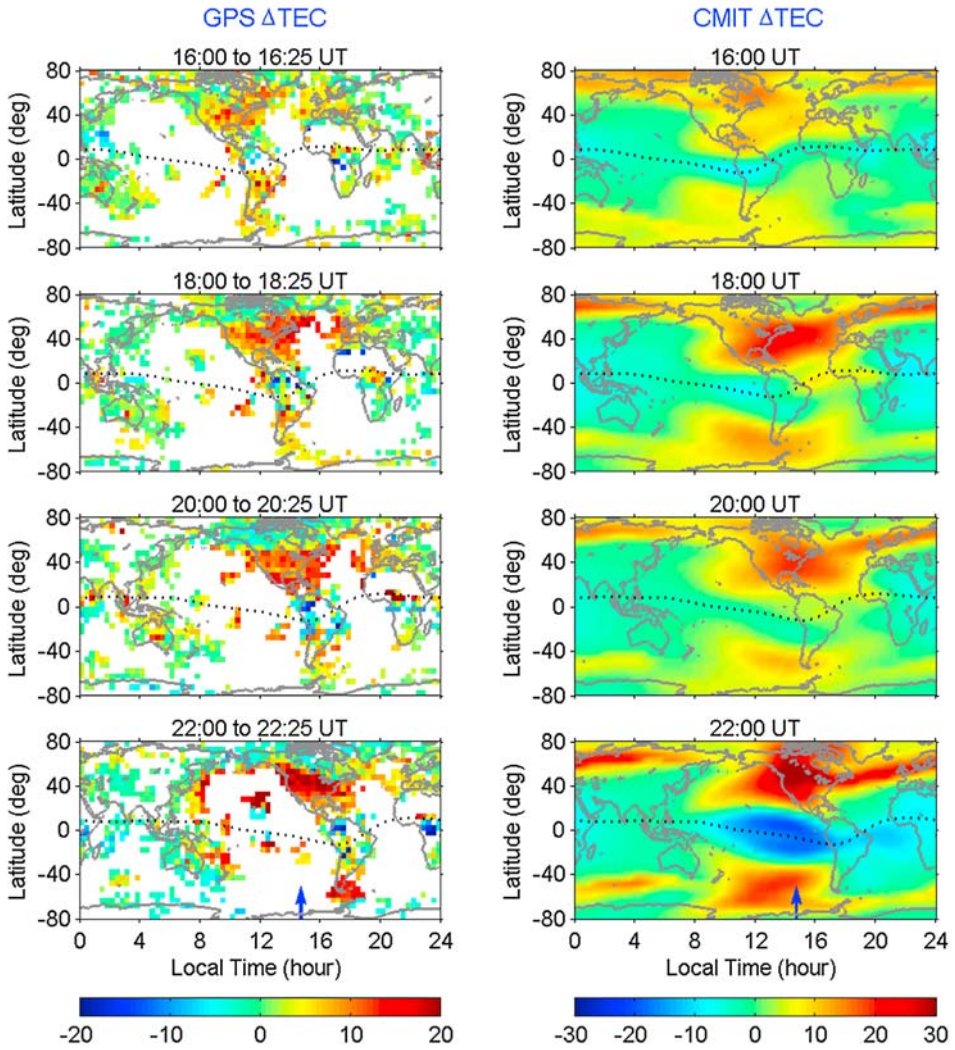

Figure 4. Same as Figure 3 but for the November 2004 storm. The disturbed day was 7 November, and quiet day was 6 November.

the right column is CMIT-simulated TEC differences between storm and quiet times. For all four UT periods shown in the figure, the CMIT results had a similar structure of global TEC enhancements to that of the observations. Positive storm effects occurred in roughly the same places in both the North and South American sectors as they did in the observations and became stronger with time. The magnitudes and temporal variations of the TEC changes simulated by the CMIT model were also very close to those observed by the ground GPS network. Negative storm effects were seen along the geomagnetic equator as well as in the high-latitude regions at later UTs in the model results: the same regions and times as those in the GPS TEC maps.

[27] There were, however, some significant differences between the model results and observations. First, the positive storm effects in the North American sector appeared to be weaker than those in the observations. Also, the modeled positive storm effects did not extend into the Europe sector at later local times. Second, it seems that the model predicted a significant hemispherically asymmetric response to the storm. Larger positive storm effects occurred in the Southern Hemisphere than in the Northern Hemisphere during daytime in the model results for this April storm, whereas the observations indicated that the northern hemisphere had a stronger positive response. There were also indications in the observations that the positive storm effect extended to the east of Australia (2200–2225 UT), which was consistent with model results. Lastly, the magnitude of the modeled negative storm response at high latitudes appeared to be weaker than that seen in the observations. This was probably the result of high-latitude Joule heating being underestimated in the model during the storm. Other processes, such as neutral wind circulation, may also affect the simulation results.

[28] Figure 4 illustrates a comparison between the modeled and observed TEC difference maps for the November 2004 storm. Note that different color scales are used in Figure 4, indicating that the model severely overestimated positive storm effects by about 50%, as well as negative storm effects in the 2200–2225 UT period. In addition, the model also clearly overestimated auroral precipitation at high latitudes with strong TEC bands caused by auroral precipitation occurring in each hemisphere. It is also evident that negative

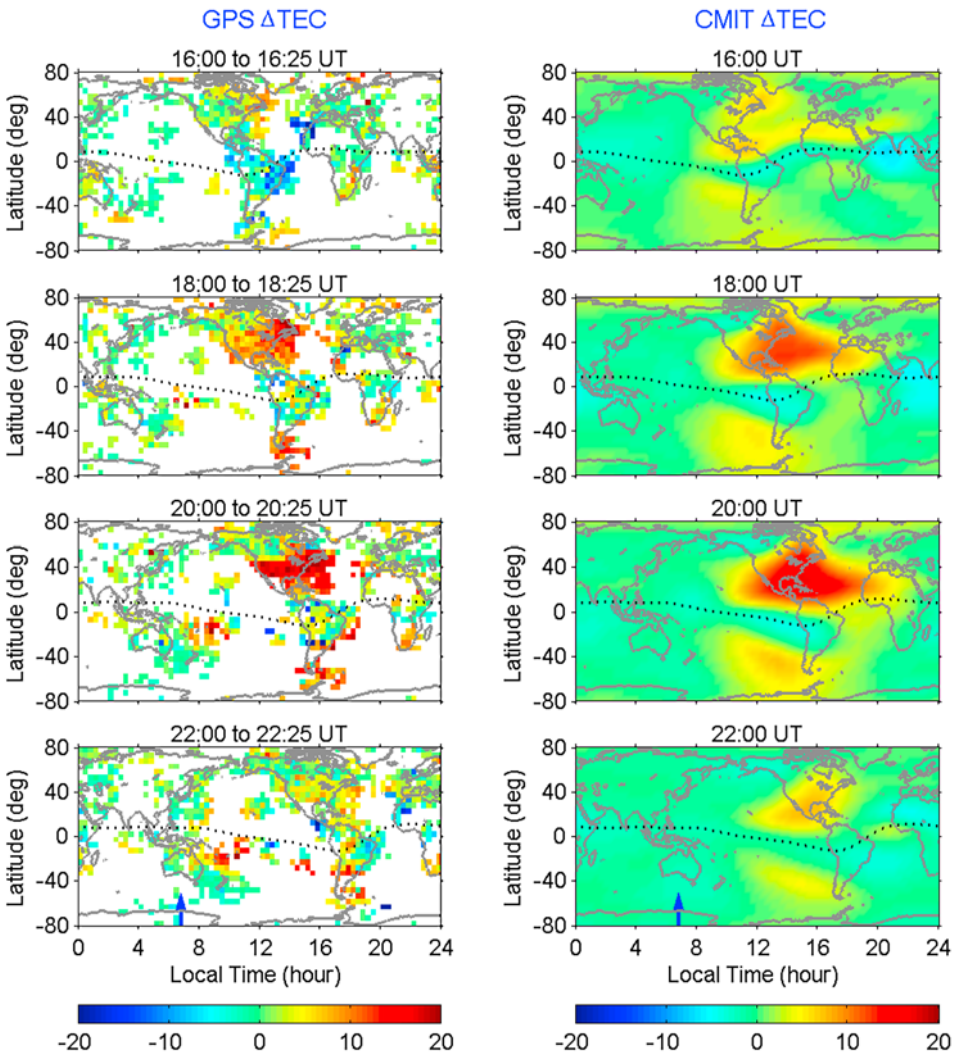

Figure 5. Same as Figure 3 but for the December 2006 storm. The disturbed day was 14 December, and quiet day was 13 December [after *Lei et al.*, 2008].

storm effects occurred at high latitudes in both hemispheres in the 2000–2025 UT and 2200–2225 UT intervals for the observed TEC maps but that this negative storm response did not happen in the model results. Despite these differences, however, the modeled global distribution and temporal variations of the positive storm effects were similar to those of the observations. In the Northern Hemisphere, the modeled positive storm effects increased as UT progressed. The morning edge of the positive storm effects occurred at about 0800 local time (LT) and stayed at that LT throughout the initial phase, in agreement with the observations. In short, positive storm effects were first seen along the west coast of the North American sector at 1600 UT but gradually expanded to near the east coast of Japan. It appears that positive storm effects extended from early morning local time, through a maximum in the early afternoon and then tapered off gradually into the evening hours. These features were almost the same as those seen in the observations. In the Southern Hemisphere, modeled positive storm effects extended from the tip of South America to the east of Australia, which was the same morphology as that seen in the observations. In addition, the model also showed a north-south asymmetry in response to the storm, with stronger positive storm effects in the Northern Hemisphere in this case. This appears to be in consistent with the observations, which also showed that Northern Hemisphere positive storm effects were stronger than those in the Southern Hemisphere, at least in the North and South American sectors.

[29] The best comparison between the model simulations and observations occurred for the December 2006 storm, as shown in Figure 5. The modeled magnitude, morphology, and time evolution of both the positive and negative storm effects were very close to the observed ones. The north-south asymmetry seen in the observations in the 1800–1825 UT and 2000–2025 UT intervals were also reproduced by the model. However, the model clearly underestimated positive storm effects in the Southern Hemisphere. The modeled TEC enhancements were smaller than the observations by about 50%, and the regions of the enhancement did not extend further west to the east coast of Australia as shown in the observed TEC maps in the later UT periods. This underestimation at this UT interval by the model might be related to a

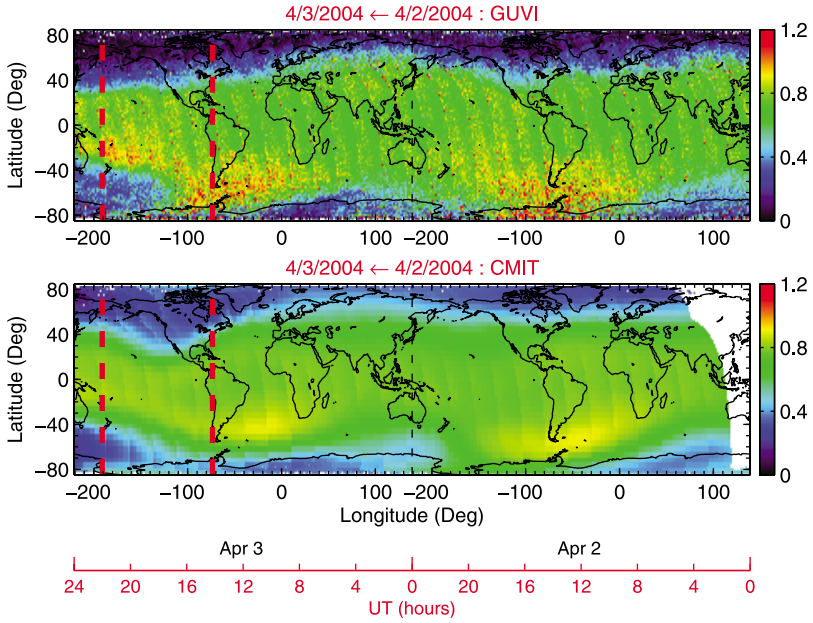

Figure 6. Global maps of (upper) O/N_2 ratio observed by GUVI and (bottom) CMIT-simulated O/N_2 ratio on 2 and 3 April 2004 in UT day (time from right to left) for a nearly constant local time of 9.3 h. The two vertical red lines indicate the time interval of the initial phase.

faster recovery from the storm effects in the model simulations, which was caused by a strong downward ambipolar diffusion and neutral wind transportation of the plasma to lower altitudes where molecular recombination is effective [*Jee et al.*, 2007]. A more detailed comparison between the observations and CMIT simulations during this event is given by *Lei et al.* [2008].

[30] In addition, in both the model results and observations, there were enhancements of TEC occurring around 1400 LT in Figures 3–5 at all UT at high middle latitudes (about ±50°) that extended to higher latitudes for all three storms. These TEC enhancements were the results of enhanced high-latitude convection patterns that transported plasma from daytime middle latitudes, across the polar cap and into the nighttime auroral region. These corresponded to a well-known phenomenon at high latitudes: the tongue of ionization, which was significantly enhanced during these storm cases [e.g., *Crowley*, 1996; *Schunk and Sojka*, 1996; *Burns et al.*, 2004b].

[31] Therefore, the CMIT model showed very similar responses of the ionosphere to the initial phases of these three storms, although there were some differences in the magnitudes and hemispheric structures of both the positive and negative storm effects. It is thus possible to investigate, by diagnostically analyzing model results, the causal mechanisms for the observations as well as the simulated common features of the ionospheric response to the initial phases of storms under different geophysical conditions.

4. Mechanisms for the Similar Ionospheric Response to the Initial Phases of the Three Storms

4.1. Negative Storm Effects

[32] Both model results and observations have shown that there were significant negative storm effects even during the initial phases of these storms. These negative storm effects occurred in two distinct regions: high to middle latitudes and along the geomagnetic equator. The mechanisms for the negative storm effects in these two regions were different. As will be discussed in detail in the next section, the negative storm effects occurring in the magnetic equatorial region were mostly related to plasma transport processes, whereas those occurring at middle and high latitudes were associated with thermospheric composition changes.

[33] It is fortunate that, during these storms, the Global Ultraviolet Imager (GUVI) instrument onboard the TIMED satellite was making observations of the ratio of atomic oxygen column densities to molecular nitrogen column densities (O/N_2) in the daytime. O/N_2 can be used as a measure of the relative importance of chemical production and loss to ionospheric plasma densities (TEC). High O/N_2 implies greater plasma production relative to chemical recombination and thus high electron densities in daytime, whereas low O/N_2 indicates that more molecular recombination and less production occurred and hence that electron densities decreased. The GUVI-measured changes of O/N_2 between storm and quiet times can thus be related to the ionospheric plasma density and TEC variations. Detailed descriptions of the GUVI instrument and data analysis procedure are given by *Christensen et al.* [2003], *Strickland et al.* [2004], and *Zhang et al.* [2004].

[34] The TIMED satellite is in a slowly precessing orbit, with an inclination of 74.1°. It takes about 2 months to rotate through 12 h of local time. Therefore, during storms that lasted 2–3 days, GUVI measurements were made in roughly the same local time plane. For the April 2004, November 2004, and December 2006 storms that we are interested in here, the local times of GUVI observations were 9.3, 14.7, and 6.8 h, respectively. These LTs are marked by arrows in the bottom two plots of Figures 3–5 for each storm, respectively.

[35] Figure 6 (top) shows GUVI-measured, global distribution of O/N_2 during the April 2004 storm at a fixed local

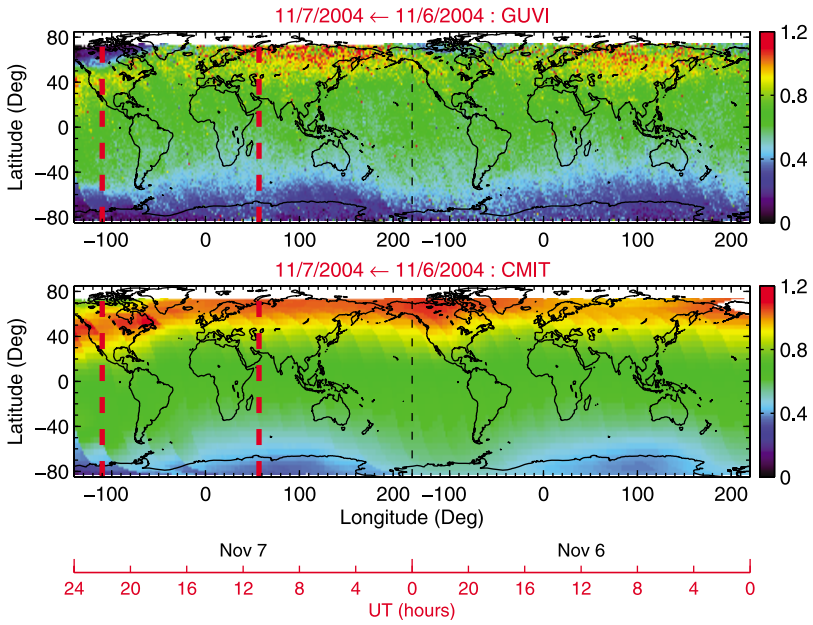

Figure 7. Same as Figure 6 but for 6 and 7 November 2004 and a nearly constant local time of 14.7 h.

time of 9.3 h. Universal time goes from right to left, and UT day is shown at the bottom of the figure. The two vertical broken red lines indicate the UT interval of the initial phase of the 3 April 2004 storm (shaded time interval in Figure 1a), for which TEC difference maps are given in Figure 3. At ~1400 UT when the initial phase began, O/N_2 on 3 April was about the same as it was on 2 April, which was a quiet day. In the following UT hours until 2000 UT, the temporal variations of O/N_2 in the storm day were different from those in the quiet day. On 2 April, the O/N_2 depleted region in the Northern Hemisphere ($O/N_2 < 0.4$) extended from high latitudes to about 45°N in the Great Lakes region. The lower boundary of this O/N_2–depleted region then gradually retreated to higher latitudes along the coast of Alaska at 2200 UT, whereas on 3 April, this depletion region moved further south to about 40°N at the same UT. In the Southern Hemisphere, O/N_2 was large at high latitudes in the UT interval between 1400 and 2000 UT on the quiet day, but it was depleted during the initial phase of the storm at later UTs.

[36] The CMIT-simulated O/N_2 at the same local time as the GUVI measurements is shown in Figure 6 (bottom) with the same color scale. The temporal variation of the simulated O/N_2 was very close to that of the observations both on 2 and 3 April, that is, high O/N_2 between about 0800 and 1800 UT in a latitudinal band around 40° in the Southern Hemisphere. However, the modeled O/N_2 appeared to be about 10%–20% less than the observed ratios. In addition, the modeled O/N_2–depletion region did not extend as far southward in the Northern Hemisphere as the observations did on 2 April but extended to too low latitudes on the disturbed day. In addition, the model also reproduced the observed O/N_2 depletion at later UTs in the Southern Hemisphere.

[37] As GUVI and the CMIT model both showed O/N_2 changes during the initial phase of the storm, we should expect that chemical processes would affect ionospheric electron densities and TEC in both the data and the model. This was clearly the case. In Figure 3 at 9.3 LT (marked with blue arrows), both ground GPS and modeled TEC maps show that negative storm effects strengthened with UT and became clearly noticeable in the Alaska-Bering Sea region as UT progressed, which was consistent with the O/N_2 changes seen in Figure 6.

[38] Figure 7 (top) gives GUVI-observed O/N_2 during the 6–9 November 2004 event and CMIT-simulated O/N_2 in Figure 7 (bottom) in the same format as Figure 6 but for 14.7 LT. The model clearly overestimated the magnitude of the O/N_2 in the Northern Hemisphere by almost a factor of 2 in most of the high-latitude regions. There were regions of depleted O/N_2 occurring after about 1800 UT and at high latitudes in both hemispheres in both the observations and simulations. In response to these storm-time O/N_2 changes, the GPS TEC difference maps also showed the development of negative storm effects at high latitudes at later UTs (Figure 4, left column). There are few or no TEC measurements over the south Pacific; thus, there is no information about whether there were TEC changes that were related to these O/N_2 variations. The model-simulated TEC maps did not show the observed negative response at high latitudes at this local time. This is probably caused by the overestimation of O/N_2 by the model.

[39] Figure 8 shows, in the same format as Figures 6 and 7, both the GUVI-observed and the CMIT model-calculated O/N_2 during the 13–16 December 2006 storm. No GUVI data were available in the Northern Hemisphere during this event. The GUVI O/N_2 can be obtained only for dayside (solar zenith angle < 90). Because of the combination of the northern winter (13–14 December) and the local time of TIMED satellite orbits during that period, the GUVI data coverage is limited to mostly Southern Hemisphere (with solar zenith angle < 90). Compared with O/N_2 on the quiet day of 13 December, large decreases in O/N_2 were seen in the Southern Hemisphere from about 1900 UT. This region of O/N_2 decreases extended further north to include Australia at 2225 UT. The modeled O/N_2 depletion, however, did not

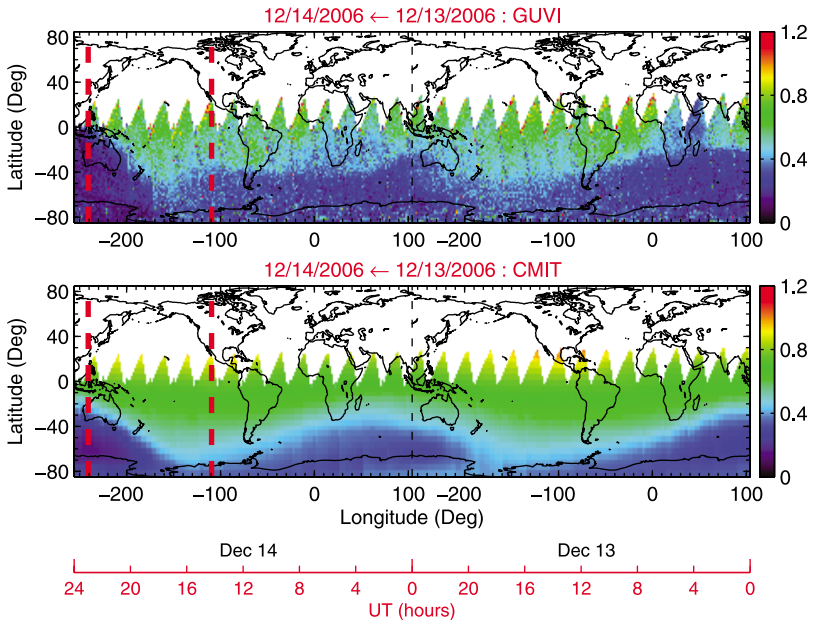

Figure 8. Same as Figure 6 but for 13 and 14 December 2006 and a nearly constant local time of 6.8 h.

extend as far north as that observed by the GUVI instrument. The TEC difference maps from both observations and model calculations that were shown in Figure 5 for the same event also had weak TEC decreases by a few TEC units in the 2000–2025 UT and 2200–2225 UT intervals in the Australian sector at the same local time as the GUVI measurements.

[40] Therefore, the negative storm response seen in the TEC maps at high latitudes and some times at middle latitudes were clearly related to the storm-time changes in O/N_2. Our results here are consistent with previous theoretical analyses and observations that have demonstrated that large-scale ionospheric electron density depletions at high and middle latitudes are caused by changes in thermospheric composition driven by intense Joule heating at high latitudes and the expansion of this disturbed composition zone by enhanced neutral wind circulation at night and in the early morning hours [e.g., *Prölss et al.*, 1991; *Prölss*, 1995; *Burns et al.*, 1995, 2007; *Strickland et al.*, 1999, 2001]. However, these large-scale negative effects mostly occurred during the main and later phases of the storms, when composition disturbances had time to develop and propagate. Our results show that such depletions can occur during the initial phase of storms, but they are confined to high latitudes in this phase. Also, the magnitudes of electron density and TEC depletions were not large because the accumulated energy inputs to the thermosphere and ionosphere were still not sufficient to drive large changes in neutral composition during this early stage of these storms. Furthermore, neutral wind circulation had also not been greatly enhanced by this stage of the storm because of the long time scale for ion-neutral coupling [*Ponthieu et al.*, 1988], so the region of depleted O/N_2 had not been advected far from the auroral oval.

[41] The negative storm effects near the geomagnetic equator did not correspond to such variations of O/N_2 during the early phases of these storms. GUVI observations as well as model simulations did not show any noticeable composition changes at lower latitudes during these times. Thus, negative storm effects along the geomagnetic equator, which happened in all three storms, must be the result of some plasma transport process. This will be considered in the next section.

4.2. Plasma Transport Effects

[42] Ionospheric F_2 region electron densities, which constitute most of TEC, are controlled by not only the chemical processes that we discussed in the previous section but also by transport processes. Transport processes are effective in changing electron densities because O^+ has a relatively long lifetime in the F_2 region. These transport processes include neutral winds, ambipolar diffusion, and ExB drift caused by ionospheric electric fields. The electric fields at low and middle latitudes include the neutral wind dynamo and penetration electric fields from high latitudes. *Wang et al.* [2008] showed that, when there was a temporal variation in the IMF B_z component, penetration electric fields occurred in low and middle latitudes. *Lei et al.* [2008] showed that, during the initial phase of the December 2006 storm, penetration electric fields were the primary cause of the observed positive TEC storm effects in the daytime. In this section we discuss if the daytime positive storm effects seen in the other two storms were also caused by penetration electric fields. We also discuss the transport processes that were responsible for the negative storm effects along the geomagnetic equator.

[43] Figure 9 shows CMIT-modeled, ionospheric zonal electric fields at Jicamarca, which is on the geomagnetic equator in the North American sector, for these storm events. The black lines are the electric fields the day before the storm for each event, whereas the red lines are the storm day electric fields. The vertical dashed lines indicate SSC times. Eastward electric fields produce upward plasma drifts at the geomagnetic equator through ExB drift. This lifts the ionosphere to higher altitudes. Ambipolar diffusion then transports plasma away from the magnetic equator, decreasing electron densities in this region [*Abdu*, 1997; *Mendillo*, 2006; *Lei et al.*,

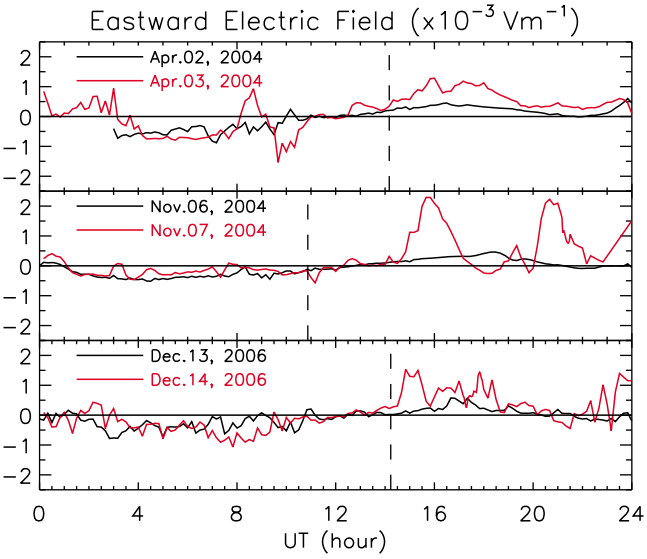

Figure 9. Eastward electric field (mVm^{-1}) at the geomagnetic equator in the North American sector (−11.9°S, 76°W, eastward positive) for (upper) April 2004, (middle) November 2004, and (bottom) December 2006 storm events, respectively. The black lines are the electric fields during the quiet times, and red lines are electric fields during the storm times. The vertical dashed lines indicate the SSC time for each storm. LT = UT − 5.

2008]. Neutral winds play a less important role at the magnetic equator. However, they can transport plasma into or away from the magnetic equator region depending on the wind direction at a particular local time. In lower latitude regions away from the geomagnetic equator, eastward electric fields also lift up the ionosphere to altitudes where the molecular recombination process is less effective, and thus, ionospheric F_2 layer electron densities and TEC are enhanced. Westward electric fields, on the other hand, result in downward plasma motion that transports plasma to lower altitudes, where fast molecular recombination decreases plasma densities. Neutral wind and ambipolar diffusion both play important roles in the overall plasma transport process at low and midlatitudes. Ambipolar diffusion acts against the changes induced by electric fields during the periods we are interested in but cannot fully compensate for them. The contribution of neutral winds is very complicated, depending on latitude and local time, it can reinforce or work against the changes caused by electric fields. The net changes in the F region electron density in daytime are the combination of all these transport processes but dominated by the effect of electric fields [*Lei et al.*, 2008].

[44] Our results suggest that the plasma enhancements seen at magnetically low and middle latitudes are associated with local plasma transport. The plasma is produced locally at lower altitudes and then uplifted to higher altitudes where they can exist for a relatively long period of time. To fully understand the origin of the plasma, however, requires a diagnostic analysis of the trajectory of a plasma flux tube in the model simulations, which will be a subject of a future study.

[45] Although solar radiation and seasons were different for these three storms, the quiet day zonal electric fields were very similar as indicated by the black lines in Figure 9. They were westward at night between about 0100 and 1100 UT (2000–0600 LT), eastward in the daytime with roughly the same magnitudes, and maximized in the early afternoon. They also changed direction from westward to eastward at dawn at about the same UT. There were short period variations at the nighttime in these zonal electric fields, most obviously on 13 December 2006 and 2 April 2004. These variations were related to penetration electric fields that were induced by the oscillations in IMF B_z. *Richmond et al.* [2003] and *Wang et al.* [2008] showed that penetration electric fields can occur even during nondisturbed, low, and moderate geomagnetic activity conditions, as long as there are changes in IMF conditions and thus high-latitude electric fields. The penetration electric fields at the magnetic equator have the same direction as those in low and midlatitudes but with a smaller magnitude [*Wang et al.*, 2008]. Thus, the direction and magnitude of the penetration electric fields at the magnetic equator can be used to qualitatively describe the transport effect of plasma at geomagnetically low and midlatitudes.

[46] Figure 9 (top) shows zonal electric fields for 2 April 2004 (quiet day, black line) and 3 April 2004 (storm day, red line), respectively. After the SSC at 1410 UT, zonal electric field was eastward and became significantly larger than its quiet day values. This enhancement of the eastward electric field became smaller after about 1930 UT, but it was still larger than its quiet day equivalent. This variation of the zonal electric field was consistent with the IMF B_z changes shown in Figure 1a (middle). That is, when the IMF B_z component was southward and varied with time, a long-duration penetration of the high-latitude electric field to lower latitudes occurred. As shown by *Wang et al.* [2008, Figure 2] for the same event, the decrease of the eastward electric field after 1930 UT was related to the neutral wind dynamo, which turned westward, reducing the net amplitude of the zonal electric field. Note that the zonal electric field shown in Figure 9 was the total electric field at the geomagnetic equator that included both the penetration electric field and neutral wind dynamo. In addition, the modeled day-to-day variability that may results from changing solar radiation and other geophysical conditions in daytime under quiet conditions was very small for all three storms; thus, the differences in eastward electric fields seen in Figure 9 were mostly the result of storm effects.

[47] The TEC response to this enhanced, storm-time, eastward electric field can be clearly seen in Figure 3. Enhanced eastward electric fields caused enhanced upward lift of the plasma at geomagnetically low and middle latitudes to higher altitudes where plasma loss by recombination is less effect, producing the simulated as well as the observed storm-time TEC enhancement. TEC enhancements were not significant in the 1600–1625 UT interval but became stronger between 1800–1825 UT and 2200–2025 UT. This corresponded to the large enhancement of the eastward electric field and hence vertical drift seen between 1600 and 1930 UT (Figure 9, top). There were no large changes between the TEC map in the 2000–2025 UT interval and that in the 2200–2225 UT interval. This is understandable since the ionospheric eastward electric field was not as strong as it was in the previous intervals, so it did not transport a significant amount of plasma to higher altitudes to further enhance plasma density there.

[48] IMF B_z had two distinct large southward periods during the initial phase of the 6–9 November 2004 storm. One occurred around 1600 UT with a B_z value of about −20 nT, and one occurred between 2000 and 2200 UT with a maximum of −35 nT. Large eastward penetration electric fields occurred with these large southward IMF B_z excursions, as illustrated in Figure 9 (middle). In between these two periods, IMF B_z was positive, and zonal electric fields were westward around 1800 UT.

[49] The time evolution of the TEC differential maps that were shown in Figure 4 was consistent with the zonal electric field changes discussed above. Storm-time TEC was significantly enhanced from 1600 to 1800 UT (top two rows in Figure 4), corresponding to the large enhancement of eastward electric field and the resulted upward plasma transportation. From 1800 to 2000 UT, we actually see a slight decrease in the storm-time TEC enhancement. This was caused by the reduction of the storm-time eastward electric field, which was smaller than the quiet-time one and even became westward during this period. Therefore, compared to the quiet-time eastward electric field, the storm-time electric field acted effectively as a westward field that transported the plasma downward and depleted electron densities. From 2000 to 2225 UT we observed a significant enhancement in storm-time TEC, relating to the large eastward electric field produced by the large southward B_z.

[50] Although the initial phase of the 6–9 November 2004 storm began at 1052 UT on 7 November with a sudden enhancement of the solar wind dynamic pressure, the IMF B_z component was northward until about 1400 UT, when large penetration electric fields and ionospheric storm effects started to occur. While not shown here, we have checked both GPS and model results before 1600 UT and found no significant TEC enhancement. This is also evident in Figure 2. In the 1600–1625 UT interval, TEC difference maps did not show big TEC enhancements compared with those in the 1800–1825 UT interval. This is understandable since, as illustrated in Figure 9, storm-time eastward electric fields began to be larger than the quiet-time ones from about 1500 UT. Thus, the build up of electron densities at geomagnetically low and middle latitudes by plasma transport did not have time to become significant. The magnitudes of the storm-time TEC enhancements were dependent on both the strength and duration of the penetrating electric field, and thus the total duration of the southward excursions of the IMF B_z component. In addition, the magnetospheric shielding effect and disturbance dynamo develop as storms progress changing the strength and duration of the penetration electric field and thus affecting the strength of daytime positive storm effect.

[51] The bottom panel in Figure 9 gives the zonal electric field for 13 December 2006 and 14 December 2006, respectively. After the SSC, the eastward zonal electric field increased rapidly and stayed larger than the quiet-time one till about 2000 UT. It then became westward for almost 1 h and then turned eastward after 2200 UT. This is consistent with the temporal variations of IMF B_z, which had three southward excursions between 1600 and 1800 UT (Figure 1c) and became northward between 1800 and 2100 UT. The TEC difference maps in Figure 5 corresponded well to these IMF B_z and zonal electric field changes. Storm-time TEC enhancements were seen in the 1600–1625 UT period and then became significantly enhanced at 1800 UT, corresponding to an enhanced eastward electric field that produced a stronger upward transport effect than in the quiet-time case. The storm-time TEC enhancement continued to build up from 1800 to 2000 UT but not as rapidly as it had during the 1600 to 1800 UT interval, since the difference between storm-time and quiet-time eastward electric fields was much larger during the earlier interval. The TEC enhancement decayed rapidly after 2000 UT. This was related to the westward electric field around 2100 UT, which transported the plasma downward and reduced electron densities.

[52] The negative responses at the geomagnetic equator can also be correlated to the transport effect by zonal electric fields and their associated vertical drifts. In this case, eastward electric fields move plasma to a higher altitude where ambipolar diffusion and neutral winds transport plasma away from the magnetic equator, decreasing electron densities in this region [*Abdu*, 1997; *Mendillo*, 2006; *Lei et al.*, 2008]. For the April 2004 storm, storm-time electric field was stronger than the quiet-time one for the entire period of the initial phase, and thus, negative storm effect became stronger with time. For the November 2004 storm, we had two periods of enhanced daytime eastward electric field during daytime. Negative storm effects were also evident during the initial phase. The model actually showed that negative effects became weaker at 2000 UT when the modeled zonal electric field was smaller than the quiet-time one, although GPS TEC difference maps showed continuous strengthening of negative storm effects at that time period. This discrepancy was probably caused by the model overestimation of electric field as discussed in the next section. Negative storm effects at the geomagnetic equator during the December 2006 storm also corresponded well the changes in zonal electric fields. As shown in Figure 5, negative storm effects were evident throughout the initial phase, which was consistent with the enhancements seen in eastward electric fields.

[53] Our observations and modeling results that show the daytime depletion of ionospheric electron density around the geomagnetic equator and enhancements in the equatorial anomaly region during the initial phase of a storm are consistent with previous results. For instance, *Adeniyi* [1986] found that the F_2 layer peak density decreased during the initial phases of storms, when the initial phases occurred in local daytime at the geomagnetically equatorial station of Ibadan (magnetic dip: 6°S). The same electron density depletions around the geomagnetic equator were also seen by *Lakshmi et al.* [1991] at Manila and Chung-Li. *Yizengaw et al.* [2006] showed that daytime TEC was enhanced at geomagnetically middle latitudes but was depleted at lower latitudes during daytime in the South American sector. Recently, *Sreeja et al.* [2009] showed that in the Indian sector, electron densities in the equatorial anomaly region can be enhanced and suppressed depending on the direction of penetration electric field from high latitudes.

4.3. North-South/Seasonal Asymmetry in the Ionospheric Response

[54] The CMIT model reproduced the observed north-south or, more appropriately, seasonal asymmetry in the two hemispheres in the ionospheric response to the initial phases of the November 2004 and December 2006 storms, with a stronger positive effect in the Northern Hemisphere. However,

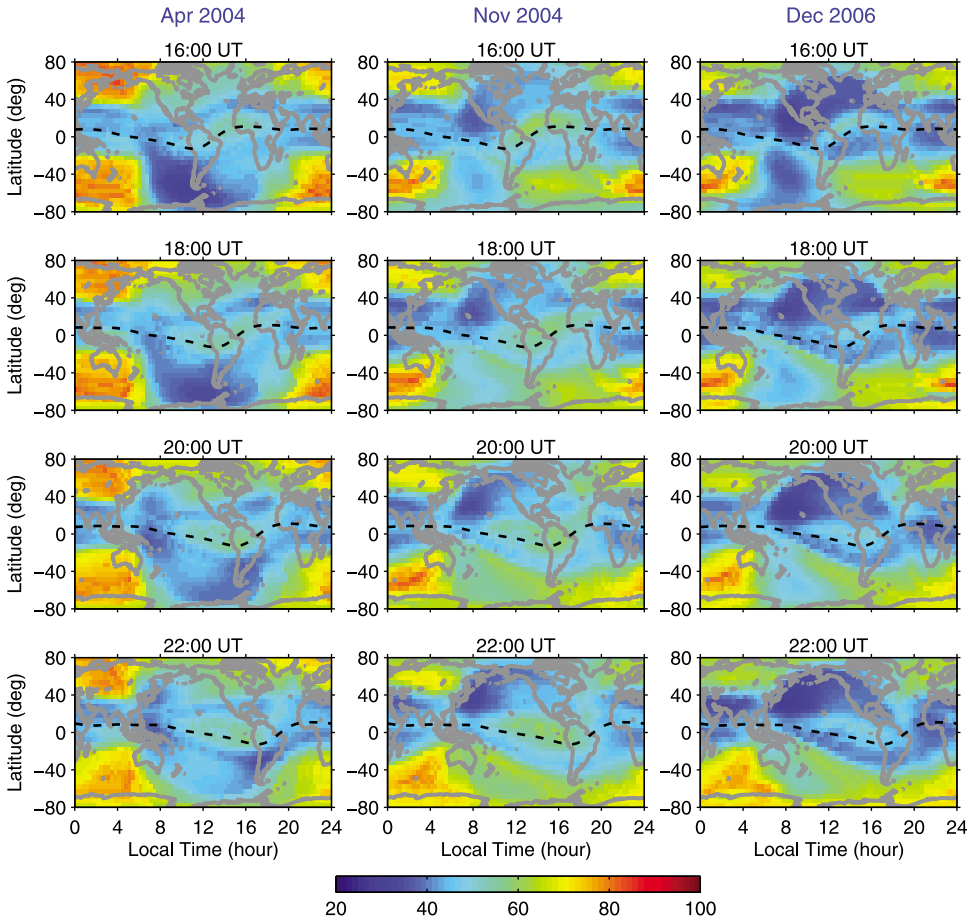

Figure 10. Global maps of the CMIT-simulated effective scale heights of the topside ionosphere (in units of kilometer) from 1600 to 2200 UT on (left) 2 April 2004, (middle) 6 November 2004, and (right) 13 December 2006, respectively. The dotted lines indicate the location of the magnetic equator.

the model did not simulate the observations well for the April 2004 storm, when the GPS TEC suggested a stronger response in the Northern Hemisphere than in the Southern Hemisphere, but the model showed the opposite structure.

[55] *Lei et al.* [2008] discussed in detail the physical processes that caused the hemispherically asymmetric response of the ionosphere for the December 2006 storm. They showed that the electron density changes caused by upward transport were related to the ratio of N_e/H_m, where N_e is the F_2 region electron density and H_m is the effective scale height of the topside ionosphere. Thus, upward transport was less effective in changing electron densities when the effective scale height was large as it was in the summer hemisphere in most places when compared to the effective scale height in the winter hemisphere at the same geomagnetic latitudes (see Figure 10). Consequently, enhancements were smaller in the summer. Therefore, for the November 2004 and December 2006 storms, the Northern (winter) Hemisphere had stronger positive responses than the Southern (summer) Hemisphere.

[56] Composition played no direct role in this seasonal asymmetry of the enhancements. Both the GUVI data and the CMIT simulations (Figures 7 and 8) showed that there were no noticeable thermospheric composition changes in the low and middle latitudes during the initial phases of these two storms, compared with the same periods during quiet time. Thus, there were no contributions to the asymmetric response by changes in thermospheric composition during the initial phases of these storms. Our results are consistent with previous observations. For instance, *Essex et al.* [1981] showed that the winter hemisphere tends to have larger TEC enhancements after storm commencement.

[57] A complication to this pattern arose in the 3–5 April 2004 storm. We have examined the ionospheric electron density profiles and effective scale heights of the CMIT model simulation for the April 2004 storm in the same way that *Lei et al.* [2008] did for the December 2006 storm. Figure 10 gives global maps of the effective scale heights near the F_2 peaks for the quiet days of these three storms. The CMIT model results for the 3 April 2004 storm (Figure 10, left) had smaller effective scale heights above the F_2 peak in the Southern Hemisphere than they did in the Northern Hemisphere, whereas, for the other two storms, the effective scale heights were all smaller in the Northern Hemisphere (winter) than in the Southern Hemisphere (summer). In addition, the quiet-time electron densities were higher in the Southern Hemisphere than in the Northern Hemisphere for the April 2004 storm event. Thus, a stronger positive response in the Southern Hemisphere occurred in the CMIT simulations, whereas the observations showed the opposite. It is currently unclear why there were such large discrepancies

between the model and data. The modeled results were consistent with conditions that were after the equinox and in at least northern hemispheric, early summer by the time of the storm, whereas data still showed northern hemispheric winter conditions.

5. Discussion

[58] Figure 9 shows that, during all three storms, long-duration, enhanced eastward electric fields occurred during day time. These eastward electric field enhancements were caused by penetration electric fields and corresponded to the periods of southward IMF illustrated in Figure 1. The long-duration penetration, as compared to the classic 20 min or so prompt penetration, has been shown recently to happen when there are temporal variations in solar wind/IMF condition and the polar cap electric fields are not steady although the penetration mechanism is the same [*Richmond et al.*, 2003; *Huang et al.*, 2005; *Huba et al.*, 2005; *Wang et al.*, 2008; *Wei et al.*, 2008]. These long-duration penetration electric fields were the most likely processes that could produces both the observed and modeled daytime TEC changes at low and middle latitudes during the initial phases of storms studied here. The long-duration penetration made it possible for plasma to be transported from lower altitudes to higher altitudes and to accumulate into significant density enhancements.

[59] There is a possibility that other processes might cause the observed changes in electron density. The first possibility is that changes in thermospheric composition associated with upwelling of molecular rich air at high latitudes caused by the intense, storm-time Joule heating and the propagation of this air to low latitudes by global neutral wind circulation. However, since both the GUVI measurements and the CMIT model simulations did not show any evidence that, in the positive response regions, there was an increase of O/N_2, the positive response was not likely related to composition changes caused by the global neutral wind circulation variations. In addition, the positive storm responses seen both in the model results and observation did not show propagating wavelike structures, and they also had much larger spatial scales (thousands of kilometers) than atmospheric gravity waves (typically about tens to hundreds of kilometers), so they were not likely associated with traveling atmospheric disturbances.

[60] Another possible cause for daytime ionospheric variations during initial phases is the neutral wind disturbance dynamo. However, the disturbance dynamo takes a long time of about 4–6 h to occur at low and middle latitudes and is normally in the westward direction in daytime [*Blanc and Richmond*, 1980; *Fejer et al.*, 1983; *Fejer and Scherliess*, 1995]. Thus, the enhanced eastward zonal electric fields in Figure 9 were caused by the penetration of high latitude electric fields to lower latitudes not by the disturbance dynamo. The daytime, westward disturbance dynamo electric field leads to a contraction of the equatorial anomaly and a decrease, instead of increase, of electron density and TEC at low and middle latitudes since westward electric fields push the ionosphere to lower altitudes where molecular recombination is more efficient [e.g. *Abdu et al.*, 1991; *Abdu*, 1997; *Sreeja et al.*, 2009]. This scenario is not consistent with both the observations and model results during the initial phases of these storms which showed that TEC and electron densities were larger, instead of smaller, at low and middle latitudes. We therefore conclude that the neutral wind dynamo is not responsible for the effects discussed in this paper.

[61] The similarity of both the middle latitude positive response and the equatorial negative response in daytime in the initial phases of these three storms was thus clearly related to the daytime zonal electric fields seen in these storms. Large storm-time, eastward penetration electric fields occurred in all three storms, which resulted in enhanced upward drifts at the geomagnetic equator leading to a depletion of electron density and TEC at the geomagnetic equator and an enhancement of electron density and TEC at geomagnetically low and middle latitudes. In daytime, high-latitude electric fields are predominately eastward when B_z is southward, and they have a very high efficiency in penetrating to middle and low latitudes. Therefore, as long as there are IMF B_z southward periods during the initial phase of geomagnetic storms, the daytime positive and negative responses of the ionosphere we see here will occur. In fact, the initial phase is usually associated with the shock arrival and the sheath period when both the solar wind and IMF are compressed by the shock, and thus, fluctuations of the IMF B_z component between northward and southward directions usually happen [e.g., *Gonzalez et al.*, 1994; *Huttunen and Koskinen*, 2004; *Zhang et al.*, 2007; *Echer et al.*, 2008]. This, in turn, means that the daytime ionospheric behavior in the initial phase that was described above should also be expected in most storms. This is consistent with previous statistical analyses of the ionospheric response during the initial phases of geomagnetic storms [e.g., *Adeniyi*, 1986].

[62] The three storms we studied here all had long initial phases. There are a significant portion of storms that have very short period of initial phases [e.g., *Gonzalez et al.*, 1994; *Huttunen and Koskinen* 2004; *Zhang et al.*, 2007; *Echer et al.*, 2008]. *Huang* [2008] carried out a case study of the 6 April 2000 storm event, which also commenced in daytime in the North American sector but had an initial phase that lasted for only about an hour. They demonstrated clearly that, in the first 2 h of the main phase, penetration electric fields were the main process that caused daytime TEC enhancements in low and middle latitudes before neutral wind circulation and composition changes propagated to lower latitudes and had a significant impact on the ionosphere. Thus, the common features of the ionospheric response to the initial phases that we demonstrated in this paper could also happen in the first few hours of the main phases of storms that have short or no initial phases, when there are similar features of eastward penetration electric fields in daytime as we showed here for the initial phases.

[63] Despite the model's general ability to describe these three storms, there were still some discrepancies in the morphology that they produced, for example, the overestimation of positive storm effects by the CMIT model during the initial phase of the 6–9 November 2004 storm. This overestimation was related to the overestimation of the penetration electric fields by the model. *Fejer et al.* [2007] described vertical ion drift velocities at the geomagnetic equator measured by the Jicamarca incoherent scatter radar during this storm: larger upward drifts occurred at around 1600 UT on 7 November, with a peak speed of about 45 m/s, corresponding to an eastward electric field of about 1 mV/m, downward drifts at about 1800 UT caused by a westward zonal electric field, and

finally another upward drift peak around 2030 UT on this day. Unfortunately, the radar did not operate after 2100 UT; thus, there were no measurements after that time. Nevertheless, an upward drift peak at 2030 UT was evident in the data. The temporal variations of these observed vertical ion drifts were very close to our modeled zonal electric fields: the CMIT results had eastward electric fields at both 1600 and 2100 UT and westward electric fields at 1800 UT. Thus, the CMIT model captured the temporal variability induced by the changes in solar wind and IMF conditions and the impact of these conditions on the thermosphere-ionosphere system. However, CMIT overestimated the magnitude of this variability. The peak values of the upward drifts in the radar measurements were 45 m/s at 1600 UT and 30 m/s at 2100 UT (roughly 1 mV/m and 0.75 mV/m at Jicamarca). But the modeled electric fields were about ~2.0 mV/s, which was about a factor of 2 larger than the observed ones. In addition, the model underestimated the westward electric field at 1800 UT also by roughly a factor of 2. The consequence of this overestimation of the eastward electric fields was an overestimation of positive storm effects (Figure 3). The CMIT model overestimated high-latitude electric fields as well as these penetration electric fields, especially for large B_z southward cases, which may be the cause of this discrepancy. The causes of this overestimation by the CMIT model have been discussed in detail by *Wang et al.* [2008]. We are currently working on improving this aspect of CMIT [*Toffoletto et al.*, 2004; *Merkin et al.*, 2007; *Wang et al.*, 2008].

6. Conclusions

[64] In this paper we have presented both ground GPS TEC observations and CMIT simulations of the global ionospheric response to the initial phases of three geomagnetic storms. Although these storms occurred in different geophysical conditions they all started at about the same universal time and had striking similarities in their early behavior. Our main findings about these storms are:

[65] 1. Positive storm effects with enhanced TEC occurred at geomagnetically low and middle latitudes in both hemispheres in daytime for all three storms. The CMIT model simulated the qualitative features of these positive storm effects well. They were caused by storm-time, eastward penetration electric fields that occurred during southward periods of IMF B_z. Eastward electric fields lift up the ionosphere to altitudes where the molecular recombination process is less effective, and thus, ionospheric F2 layer electron densities and TEC are enhanced. The model showed that storm-time TEC enhancements occurred when there were enhancements in eastward electric fields. TEC enhancements built up during these southward excursions only. The magnitudes of the enhancements were dependent on both the strength of the penetrating electric field and the total duration of the southward excursions. This effect only occurs in the daylight hours, when southward B_z produces eastward penetration electric field and hence upward ExB drifts.

[66] 2. Negative storm effects occurred along the geomagnetic equator. This depletion of electron densities was related to the transport of plasma upward by the enhanced storm-time eastward electric field and then away from the geomagnetic equator region to geomagnetically low and middle latitudes by ambipolar diffusion and neutral winds. GUVI measurements show that these negative storm effects were not associated with thermospheric composition changes.

[67] 3. Negative storm effects also happened at high latitudes for all three storms. They occurred in middle and high latitudes at night and in the early morning hours but were limited to high latitudes in daytime. They expanded to lower latitudes as the storms progressed. These electron density depletions were correlated very well with the O/N_2 decreases observed by the TIMED/GUVI instrument during the initial phases of these storms. The CMIT model did well in simulating both the composition and electron density changes seen in the observations. The composition perturbations and their associated negative storm effects were limited to high latitudes because in the early phase of storms the neutral wind circulation has not been enhanced greatly and did not have time to transport these perturbations to lower latitudes.

[68] 4. Significant north-south asymmetries in the ionospheric response were found in both the observations and model simulations for November 2004 and December 2006 storms. For these two storms, it appears that the winter hemisphere had a stronger positive response than the summer hemisphere did. The model reproduced the observed north-south, or more accurately, summer-winter asymmetries in the ionospheric response. The summer-winter asymmetry is related to the scale height and quiet-time electron density differences between winter and summer. For the same magnitude of uplifting, the summer hemisphere has a weaker response since it has a larger scale height. The April 2004 storm occurred in equinox conditions. The TEC observations showed a stronger positive ionospheric response in the Northern Hemisphere than in the Southern Hemisphere. It is currently not clear what processes caused this north-south asymmetry in the ionospheric response and the reason that the CMIT model did not simulate the observed north-south asymmetry under these equinox conditions.

[69] The similarity in the ionospheric response to the initial phases of different storms under different geophysical conditions is related to the prompt response of the global ionospheric electric field to changes in solar wind and IMF conditions. Within a couple of hours of changes in the zonal electric fields, the build up (positive response) or depletion (negative response) of ionospheric electron density occurs. Large-scale changes in neutral wind circulation and composition in response to energy and momentum inputs from the magnetosphere and solar wind/IMF require a longer response time; thus, their effects are usually confined to high-latitude auroral regions during the initial phases of the storms. Therefore, the ionospheric response at low and middle latitudes during storm initial phases is dominated by penetration electric fields. Consequently, if we know how penetration electric fields relate to IMF conditions, we can make reasonably good prediction of the ionospheric electron density response in the first few hours of storms at low and middle latitudes. This paper discusses the behavior of storms that happen at roughly the same UT. In a future study, we will study the effect of commencement time on the ionospheric response.

[70] **Acknowledgments.** This material is based upon work supported in part by NASA grants NNH08AH37I and NNX08AQ91G and by the Center for Integrated Space Weather Modeling (CISM) which is funded by the STC Program of the National Science Foundation under agreement

ATM-0120950. This work is also supported by the National Science Foundation of China (40828003). The National Center for Atmospheric Research is sponsored by the National Science Foundation. We are also grateful to Delores Knipp and Tim Fuller-Rowell for helpful discussions.

[71] Zuyin Pu thanks the reviewers for their assistance in evaluating 2009JA014461.

References

Abdu, M. A. (1997), Major phenomena of the equatorial ionosphere-thermosphere system under disturbed conditions, *J. Atmos. Sol. Terr. Phys.*, *59*, 1505–1519.

Abdu, M. A., J. H. A. Sobral, E. R. de Paula, and I. S. Batista (1991), Magnetospheric disturbance effects on the Equatorial Ionization Anomaly (EIA): An overview, *J. Atmos. Sol. Terr. Phys.*, *53*, 757–771.

Abdu, M. A., I. S. Batista, G. O. Walker, J. H. A. Sobral, N. B. Trivedi, and E. R. de Paula (1995), Equatorial ionospheric electric fields during magnetospheric disturbances: Local time/longitude dependences from recent EITS campaigns, *J. Atmos. Terr. Phys.*, *57*, 1065–1083.

Acuña, M. H., et al. (1995), The Global Geospace Science Program and its investigations, *Space Sci. Rev.*, *71*, 5.

Adeniyi, J. O. (1986), Magnetic storm effects on the morphology of the equatorial F_2 layer, *J. Atmos. Terr. Phys.*, *48*, 695–702.

Blagoveshchensky, D. V., M. Lester, V. A. Kornienko, I. I. Shagimuratov, A. J. Stocker, and E. M. Warrington (2005), Observations by the CUTLASS radar, HF Doppler, oblique ionospheric sounding, and TEC from GPS during a magnetic storm, *Ann. Geophys.*, *23*, 1697–1709.

Blanc, M., and A. D. Richmond (1980), The ionospheric disturbance dynamo, *J. Geophys. Res.*, *85*, 1669–1686.

Buonsanto, M. J. (1999), Ionospheric storms-a review, *Space Sci. Rev.*, *88*, 563–601.

Burns, A. G., T. L. Killeen, and R. G. Roble (1991), A theoretical study of thermospheric composition perturbations during an impulsive geomagnetic storm, *J. Geophys. Res.*, *96*, 14,153–14,167, doi:10.1029/91JA00678.

Burns, A. G., T. L. Killeen, W. Deng, G. R. Carignan, and R. G. Roble (1995), Geomagnetic storm effects in the low- to middle-latitude upper thermosphere, *J. Geophys. Res.*, *100*, 14,673–14,691.

Burns, A. G., T. L. Killeen, W. Wang, and R. G. Roble (2004a), The solar cycle-dependent response of the thermosphere to geomagnetic storms, *J. Atmos. Sol. Terr. Phys.*, *66*, 1–14.

Burns, A. G., W. Wang, T. L. Killeen, and S. C. Solomon (2004b), A "tongue" of neutral composition, *J. Atmos. Sol. Terr. Phys.*, *66*, 1457–1468.

Burns, A. G, S. C. Solomon, W. Wang, and T. L. Killeen (2007), The ionospheric and thermospheric response to CMEs: Challenges and successes, *J. Atmos. Sol. Terr. Phys.*, *69*, 77–85.

Cander, L. R., and S. J. Mihajlovic (2005), Ionospheric spatial and temporal variations during the 29–31 October 2003 storm, *J. Atmos. Sol. Terr. Phys.*, *67*, 1118–1128.

Christensen, A. B., et al. (2003), Initial observations with the Global Ultraviolet Imager (GUVI) in the NASA TIMED satellite mission, *J. Geophys. Res.*, *108*(A12), 1451, doi:10.1029/2003JA009918.

Crowley, G. (1996), Critical review on ionospheric patches and blobs, in *The Review of Radio Science 1992–1996*, edited by W. Stone, pp. 619–648, Oxford University Press, Oxford.

Echer, E., W. D. Gonzalez, B. T. Tsurutani, and A. L. C. Gonzalez (2008), Interplanetary conditions causing intense geomagnetic storms ($Dst \leq -100$ nT) during solar cycle 23 (1996–2006), *J. Geophys. Res.*, *113*, A05221, doi:10.1029/2007JA012744.

Essex, E. A, et al. (1981), A global response of the total electron content of the ionosphere to the magnetic storm of l7 and l8 June 1972, *J. Atmos. Terr. Phys.*, *43*, 293–306.

Fejer, B. G., and L. Scherliess (1995), Time-dependent response of equatorial ionospheric electric-fields to magnetospheric disturbances, *Geophys. Res. Lett.*, *22*, 851–854.

Fejer, B. G., M. F. Larsen, and D. T. Farley (1983), Equatorial disturbance dynamo electric fields, *Geophys. Res. Lett.*, *10*, 537–540.

Fejer, B. G., J. W. Jensen, T. Kikuchi, M. A. Abdu, and J. L. Chau (2007), Equatorial ionospheric electric fields during the November 2004 magnetic storm, *J. Geophys. Res.*, *112*, A10304, doi:10.1029/2007JA012376.

Field, P. R., H. Rishbeth, R. J. Moffett, D. W. Wenden, T. J. Fuller-Rowell, G. H. Millward, and A. D. Aylward (1998), Modelling composition changes in F-layer storms, *J. Atmos. Sol. Terr. Phys.*, *60*, 523–543.

Fuller-Rowell, T. J., M. V. Codrescu, R. J. Moffett, and S. Quegan (1994), Response of the thermosphere and ionosphere to geomagnetic storms, *J. Geophys. Res.*, *99*, 3893–3914.

Gonzalez, W. D., J. A. Joselyn, Y. Kamide, H. W. Kroehl, G. Rostoker, B. T. Tsurutani, and V. M. Vasyliunas (1994), What is a geomagnetic storm?, *J. Geophys. Res.*, *99*, 5771–5792.

Huang, C.-S. (2008), Global characteristics of ionospheric electric fields and disturbances during the first hours of magnetic storms, *Adv. Space Res.*, *41*, 527–538.

Huang, C.-S., J. C. Foster, and M. C. Kelley (2005), Long-duration penetration of the interplanetary electric field to the low-latitude ionosphere during the main phase of magnetic storms, *J. Geophys. Res.*, *110*, A11309, doi:10.1029/2005JA011202.

Huba, J. D., G. Joyce, S. Sazykin, R. Wolf, and R. Spiro (2005), Simulation study of penetration electric field effects on the low- to midlatitude ionosphere, *Geophys. Res. Lett.*, *32*, L23101, doi:10.1029/2005GL024162.

Huttunen, K., and H. Koskinen (2004), Importance of post-shock streams and sheath region as drivers of intense magnetospheric storms and high-latitude activity, *Ann. Geophys.*, *22*, 1729–1738.

Jakowski, N., A. Jungstand, K. Schlegel, H. Kohl, and K. Rinnert (1992), The ionospheric response to perturbation electric-fields during the onset phase of geomagnetic storms, *Can. J. Phys.*, *70*, 575–581.

Jee, G., A. G. Burns, W. Wang, S. C. Solomon, R. W. Schunk, L. Scherliess, D. C. Thompson, J. J. Sojka, and L. Zhu (2007), Duration of an ionospheric data assimilation initialization of a coupled thermosphere-ionosphere model, *Space Weather*, *5*, S01004, doi:10.1029/2006SW000250.

Lakshmi, D. R., B. C. N. Rao, A. R. Jain, M. K. Goel, and B. M. Reddy (1991), Response of equatorial and low latitude F region to the great magnetic storm of 13 March 1989, *Ann. Geophys.*, *9*, 286–290.

Lei, J., W. Wang, A. G. Burns, S. C. Solomon, A. D. Richmond, M. Wiltberger, L. P. Goncharenko, A. Coster, and B. W. Reinisch (2008), Observations and simulations of the ionospheric and thermospheric response to the December 2006 geomagnetic storm: Initial phase, *J. Geophys. Res.*, *113*, A01314, doi:10.1029/2007JA012807.

Lin, C. H., A. D. Richmond, J. Y. Liu, H. C. Yeh, L. J. Paxton, G. Lu, H. F. Tsai, and S.-Y. Su (2005), Large-scale variations of the low-latitude ionosphere during the October–November 2003 superstorm: Observational results, *J. Geophys. Res.*, *110*, A09S28, doi:10.1029/2004JA010900.

Lyon, J. G., J. A. Fedder, and C. M. Mobarry (2004), The Lyon-Fedder-Mobarry (LFM) global MHD magnetospheric simulation code, *J. Atmos. Sol. Terr. Phys.*, *66*, 1333–1350.

Mannucci, A. J., B. T. Tsurutani, B. A. Iijima, A. Komjathy, A. Saito, W. D. Gonzalez, F. L. Guarnieri, J. U. Kozyra, and R. Skoug (2005), Dayside global ionospheric response to the major interplanetary events of October 29–30, 2003 "Halloween Storms," *Geophys. Res. Lett.*, *32*, L12S02, doi:10.1029/2004GL021467.

Mayr, H. G., I. Harris, and N. W. Spencer (1978), Some properties of upper atmosphere dynamics, *Rev. Geophys.*, *16*, 539–565.

Mendillo, M. (2006), Storms in the ionosphere: Patterns and processes for total electron content, *Rev. Geophys.*, *44*, RG4001, doi:10.1029/2005RG000193.

Merkin, V. G., M. J. Owens, H. E. Spence, W. J. Hughes, and J. M. Quinn (2007), Predicting magnetospheric dynamics with a coupled Sun-to-Earth model: Challenges and first results, *Space Weather*, *5*, S12001, doi:10.1029/2007SW000335.

Ponthieu, J.-J., T. L. Killeen, K.-M. Lee, G. R. Carignan, W. R. Hoegy, and L. H. Brace (1988), Ionosphere-thermosphere momentum coupling at solar maximum and solar minimum from DE-2 and AE-C data, *Phys. Scr.*, *37*, 447, doi:10.1088/0031-8949/37/3/028.

Prölss, G. W. (1993), Common origin of positive ionospheric storms at middle latitudes and the geomagnetic activity effect at low latitudes, *J. Geophys. Res.*, *98*, 5981–5991.

Prölss, G. W. (1995), Ionospheric F region storms, in *Handbook of Atmospheric Electrodynamics*, vol. 2, edited by H. Volland, pp. 195–248, CRC Press, Boca Raton, Fla.

Prölss, G. W., L. H. Brace, H. G. Mayr, G. R. Carignan, T. L. Killeen, and J. A. Klobuchar (1991), Ionospheric storm effects at subauroral latitudes-a case study, *J. Geophys. Res.*, *96*, 1275–1288.

Rasmussen, C. E., and M. E. Greenspan (1993), Plasma transportation in the equatorial ionosphere during the great magnetic storm of March 1989, *J. Geophys. Res.*, *98*, 285–292.

Richmond, A. D., et al. (1980), An empirical model of quiet-day ionospheric electric fields at middle and low latitudes. *J. Geophys. Res.*, *85*, 4658–4667.

Richmond, A. D., E. C. Ridley, and R. G. Roble (1992), A thermosphere/ionosphere general circulation model with coupled electrodynamics, *Geophys. Res. Lett.*, *19*, 601–604.

Richmond, A. D., C. Peymirat, and R. G. Roble (2003), Long-lasting disturbances in the equatorial ionospheric electric field simulated with a coupled magnetosphere-ionosphere-thermosphere model, *J. Geophys. Res.*, *108*(A3), 1118, doi:10.1029/2002JA009758.

Rideout, W., and A. Coster (2006), Automated GPS processing for global total electron content data, *GPS Solutions*, 10, 219–228, doi:10.1007/s10291-006-0029-5.

Roble, R. G., E. C. Ridley, A. D. Richmond, and R. E. Dickinson (1988), A coupled thermosphere/ionosphere general circulation model, *Geophys. Res. Lett.*, *15*, 1325–1328.

Romanova, E. B., O. M. Pirog, N. M. Polekh, A. V. Tashchilin, G. A. Zherebtsov, J. K. Shi, and X. Wang (2008), Modeling of ionospheric parameter variations in East Asia during the moderate geomagnetic disturbances, *Adv. Space Res.*, *41*, 569–578.

Schunk, R. W., and J. J. Sojka (1996), Ionosphere-thermosphere space weather issues, *J. Atmos. Sol. Terr. Phys.*, *58*, 1527–1574.

Sreeja, V., C. V. Devasia, Sudha Ravindran, Tarun Kumar Pant, and R. Sridharan (2009), Response of the equatorial and low-latitude ionosphere in the Indian sector to the geomagnetic storms of January 2005, *J. Geophys. Res.*, *114*, A06314, doi:10.1029/2009JA014179.

Stone, E. C., A. M. Fransden, R. A. Mewaldt, E. R. Christian, D. Margolies, J. F. Ormes, and F. Snow (1998), The Advanced Composition Explorer, *Space Sci. Rev.*, *86*, 1.

Strickland, D. J., R. J. Cox, R. R. Meier, and J. D. Craven (1999), Global O/N_2 derived from DE-1 FUV imaging dayglow data: Technique and examples from two storm periods, *J. Geophys. Res.*, *104*, 4251–4266.

Strickland, D. J., J. D. Craven, and R. E. Daniell (2001), Six days of thermospheric-ionospheric weather over the Northern Hemisphere in late September 1981, *J. Geophys. Res.*, *106*, 30,291–30,306.

Strickland, D. J., R. R. Meier, R. L. Walterscheid, J. D. Craven, A. B. Christensen, L. J. Paxton, D. Morrison, and G. Crowley (2004), Quiet-time seasonal behavior of the thermosphere seen in the far ultraviolet dayglow, *J. Geophys. Res.*, *109*, A01302, doi:10.1029/2003JA010220.

Swisdak, M., J. D. Huba, G. Joyce, and C.-S. Huang (2006), Simulation study of a positive ionospheric storm phase observed at Millstone Hill, *Geophys. Res. Lett.*, *33*, L02104, doi:10.1029/2005GL024973.

Szuszczewicz, E. P., M. Lester, P. Wilkinson, P. Blanchard, M. Abdu, R. Hanbaba, K. Igarashi, S. Pulinets, and B. M. Reddy (1998), A comparative study of global ionospheric responses to intense magnetic storm conditions, *J. Geophys. Res.*, *103*, 11,665–11,684.

Toffoletto, F. R., S. Sazykin, R. W. Spiro, R. A. Wolf, and J. G. Lyon (2004), RCM meets LFM: Initial results of one-way coupling, *J. Atmos. Sol. Terr. Phys.*, *66*, 1361–1370.

Wang, W., M. Wiltberger, A. G. Burns, S. C. Solomon, T. L. Killeen, N. Maruyama, and J. Lyon (2004), Initial results from the CISM coupled magnetosphere ionosphere thermosphere (CMIT) model: Thermosphere ionosphere responses, *J. Atmos. Sol. Terr. Phys.*, *66*, 1425–1441.

Wang, W., J. Lei, A. G. Burns, M. Wiltberger, A. D. Richmond, S. C. Solomon, T. L. Killeen, E. R. Talaat, and D. N. Anderson (2008), Ionospheric electric field variations during a geomagnetic storm simulated by a coupled magnetosphere ionosphere thermosphere (CMIT) model, *Geophys. Res. Lett.*, *35*, L18105, doi:10.1029/2008GL035155.

Wei, Y., M. Hong, W. Wan, A. Du, J. Lei, B. Zhao, W. Wang, Z. Ren, and X. Yue (2008), Unusually long-lasting multiple penetration of interplanetary electric field to equatorial ionosphere under oscillating IMF Bz, *Geophys. Res. Lett.*, *35*, L02102, doi:10.1029/2007GL032305.

Wiltberger, M., W. Wang, A. Burns, S. Solomon, J. G. Lyon, and C. C. Goodrich (2004), Initial results from the coupled magnetosphere ionosphere thermosphere model: Magnetospheric and ionospheric responses, *J. Atmos. Sol.-Terr. Phys.*, *66*, 1411–1423.

Yizengaw, E., M. B. Moldwin, A. Komjathy, and A. J. Mannucci (2006), Unusual topside ionospheric density response to the November 2003 superstorm, *J. Geophys. Res.*, *111*, A02308, doi:10.1029/2005JA011433.

Zhang, J., et al. (2007), Solar and interplanetary sources of major geomagnetic storms ($Dst \leq 100$ nT) during 1996–2005, *J. Geophys. Res.*, *112*, A10102, doi:10.1029/2007JA012321.

Zhang, Y., L. J. Paxton, D. Morrison, B. Wolven, H. Kil, C.-I. Meng, S. B. Mende, and T. J. Immel (2004), O/N_2 changes during 1–4 October 2002 storms: IMAGE SI-13 and TIMED/GUVI observations, *J. Geophys. Res.*, *109*, A10308, doi:10.1029/2004JA010441.

Zhao, B, W. Wan, and L. Liu (2005), Responses of equatorial anomaly to the October–November 2003 superstorms, *Ann Geophys.*, *23*, 693–706.

A. G. Burns, S. C. Solomon, W. Wang, and M. Wiltberger, High Altitude Observatory, National Center for Atmospheric Research, PO Box 3000, Boulder, CO 80307-3000, USA. (wbwang@ucar.edu)

A. Coster, Haystack Observatory, Massachusetts Institute of Technology, Westford, MA 01886, USA.

J. Lei, Aerospace Engineering Sciences Department, University of Colorado at Boulder, Boulder, CO 80309, USA.

L. Paxton and Y. Zhang, Applied Physics Laboratory, Johns Hopkins University, Laurel, MD 20723, USA.

J. Xu, State Key Laboratory of Space Weather, Chinese Academy of Sciences, Beijing 100080, China.